

Reduction of short wavelength reflectance of multi-wall carbon nanotubes through ultraviolet laser irradiation

Michelle S. Stephens, Brian J. Simonds, Christopher S. Yung, Davis Conklin, David J. Livigni, Alberto Remesal Oliva, and John H. Lehman

Citation: *AIP Advances* **8**, 055229 (2018); doi: 10.1063/1.5021263

View online: <https://doi.org/10.1063/1.5021263>

View Table of Contents: <http://aip.scitation.org/toc/adv/8/5>

Published by the [American Institute of Physics](#)

Articles you may be interested in

[Carbon nanotube-based black coatings](#)

Applied Physics Reviews **5**, 011103 (2018); 10.1063/1.5009190

AIP | Conference Proceedings

Get **30% off** all
print proceedings!

Enter Promotion Code **PDF30** at checkout



Reduction of short wavelength reflectance of multi-wall carbon nanotubes through ultraviolet laser irradiation

Michelle S. Stephens,^{1,a} Brian J. Simonds,¹ Christopher S. Yung,¹
Davis Conklin,¹ David J. Livigni,¹ Alberto Remesal Oliva,²
and John H. Lehman¹

¹National Institute of Standards and Technology, 325 Broadway, Boulder, CO 80305, USA

²Physikalisch-Meteorologisches Observatorium Davos, World Radiation Center,
Dorfstrasse 33, 7260 Davos Dorf, Switzerland

(Received 2 January 2018; accepted 18 May 2018; published online 29 May 2018)

Multi-wall carbon nanotube coatings are used as broadband, low-reflectance absorbers for bolometric applications and for stray light control. They are also used as high emittance blackbody radiators. Irradiation of single wall carbon nanotubes with ultraviolet (UV) laser light has been shown to remove amorphous carbon debris, but there have been few investigations of the interaction of UV light with the more complex physics of multi-wall carbon nanotubes. We present measurements of reflectance and surface morphology before and after exposure of multi-wall carbon nanotube coatings to 248 nm UV laser light. We show that UV exposure reduces the reflectivity at wavelengths below 600 nm and present modeling of the thermal cycling the UV exposure causes at the surface of the carbon nanotubes. This effect can be used to flatten the spectral shape of the reflectivity curve of carbon nanotube absorber coatings used for broadband applications. Finally, we find that the effect of UV exposure depends on the nanotube growth process. © 2018 Author(s). All article content, except where otherwise noted, is licensed under a Creative Commons Attribution (CC BY) license (<http://creativecommons.org/licenses/by/4.0/>). <https://doi.org/10.1063/1.5021263>

I. INTRODUCTION

Carbon nanotube-based black absorbers are increasingly being used as optically black surfaces for absolute radiometric measurements with pyroelectric detectors¹ and bolometers for laser power,^{2,3} solar irradiance,⁴ and Earth radiance.⁵ They are also used for blackbody radiators^{6,7} and stray light control.^{8,9} They are of particular value for these applications because they are very low reflectance (and therefore high absorptivity and emissivity) over a broader wavelength range than any other black coatings.^{10,11} The reflectance, although still low, begins to increase at wavelengths below 600 nm.¹² Many applications that require a spectrally flat absorber would benefit from being able to further reduce the reflectance at these shorter wavelengths. Furthermore, knowledge of if and how the reflectance of these absorbers change in the harsh environment of space or direct sunshine over time is important to maintain a low uncertainty in all such applications. Therefore, an understanding of how environmental exposure such as UV irradiation influences the reflectance of the absorber is needed.

Measurements have been reported on the use of ultraviolet laser irradiation to purify single wall carbon nanotubes and on the nature of their morphology,^{13,14} however, the influence of ultraviolet laser irradiation on the reflectance of very dark carbon nanotube absorbers has not been explored.

In this work, we study the influence of UV exposure on multi-wall carbon nanotube (CNT) absorbers' surface morphology and absorptivity by irradiating samples in vacuum with a 248 nm quasi-cw laser. We compare samples that have been prepared on different surfaces and with different

^aElectronic mail: michelle.stephens@nist.gov

carbon nanotube growth processes. We show that reflectivity at short wavelengths can be reduced with UV laser irradiation. The influence of the UV exposure differs for different sample types. For each, the UV exposure creates an initial drop in reflectance at short wavelengths, while the outcome of extended exposure varies.

Finally, we discuss different physical mechanisms for the interaction of the UV laser light with the CNTs and how they may be affecting the reflectivity of the samples.

II. EXPERIMENTAL

Three nanotube absorber samples were measured. Two were samples of commercially available carbon nanotubes on Al substrates (40 mm x 40 mm). One commercial sample was a spray-on coating consisting of non-aligned CNTs mixed with a binder. The spray-on coating is a low temperature deposition process at approximately 100 °C. The other commercial sample consisted of vertically aligned carbon nanotubes (VACNTs) grown (450 °C process) on an Al substrate to a height of approximately 30 μm. The third sample consisted of 450 μm long VACNTs grown at NIST on a 40 mm diameter SiO₂ passivated Si substrate using a plasma enhanced chemical vapor deposition (PE-CVD) process at 800 °C.^{15,16}

A. Laser exposure

Figure 1 shows a schematic of the measurement. Laser exposure of CNT absorbers was carried out using a pulsed KrF excimer laser at 248 nm. The sample under test was mounted in a vacuum system with a residual pressure of < 0.05 Pa. The sample was mounted to an optical post that was heat sunk to the vacuum base. A type K thermocouple was mounted near the back of the substrate monitored the temperature of the sample during laser irradiation. The 248-nm laser entered the vacuum system through a CaF₂ optical window.

Samples were irradiated with laser pulses with energy $E = 21.4 \pm 2.72$ mJ/pulse to build up the cumulative exposure. The samples were periodically removed and characterized, then returned for additional irradiation. Smaller UV exposure increments were used on the spray-on coating because it was apparently less robust.

The laser pulse duration, τ , was 22 ns (full width at half maximum), and the pulse repetition rate, ν , was set to 200 pulses/s. After transmission through the aperture, the laser beam spatial distribution was a circular top-hat beam with diameter $d = 1.3$ cm. The peak power density, $P_{peak} = \frac{4E}{\pi\tau d^2} = 0.73$ MW/cm² and the average power density $P_{average} = \frac{4E\nu}{\pi d^2} = 3.2$ W/cm².

As the samples were irradiated, the temperature of the samples rose. When the substrate temperature rose to greater than 85 °C, the experiment was paused until the sample cooled to below 25 °C.

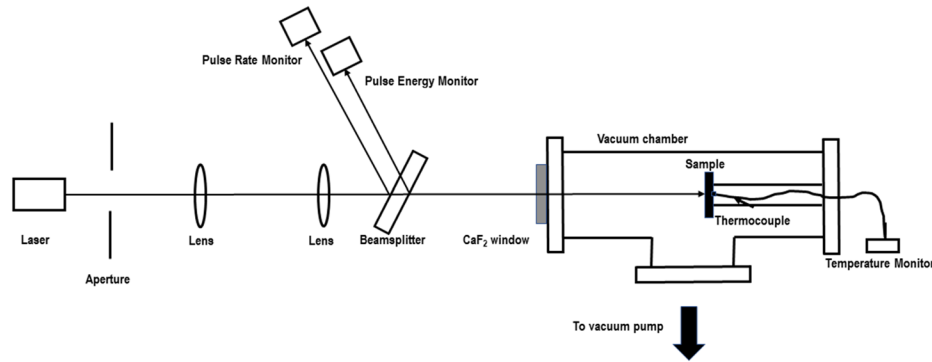


FIG. 1. Layout of the optical setup. A pulsed 248 nm excimer laser is apodised by a circular aperture, then collimated to a beam diameter of 1.3 cm. A pick-off beamsplitter sends signals to two detectors, one that acts as a pulse energy monitor and another that acts as a pulse rate monitor. The remaining light passes through a CaF₂ window into the vacuum system and is incident on the carbon nanotube absorber. The pulse energy at the sample is 20 mJ, and the pulse energy at the monitor is 1.3 mJ.

The temperature of the top surface of the nanotubes was likely much hotter. This effect is discussed in Section IV.

Each carbon nanotube sample was characterized before and after irradiation with field emission scanning electron microscopy (FESEM) and total hemispherical reflectance measurements.

B. Pre- and post-exposure characterization

The reflectivity of the samples from 300 to 2000 nm was measured before UV exposure and after several different UV exposure durations for each sample. A commercial monochromator-based spectrophotometer with a 150 mm diameter integrating sphere was used. Absolute reflectance values were determined by using a commercially available, calibrated reflectance standard made from a similar material to the sphere wall. Expanded relative uncertainties ($k = 2$) in the measured spectral range from roughly 10% to 100% depending on the value of the reflectance. This is primarily due to deterioration of the signal-to-noise ratio as the samples become more absorptive.

Imaging of the surface of the absorbers by FESEM before UV exposure and after several different UV exposure durations for each sample provided a qualitative measure of UV induced morphological changes. Changes in the surface morphology of VACNT samples has been shown to affect their reflectivity.^{11,16}

III. RESULTS

All three coatings show a reduction in reflectance at wavelengths below 600 nm after UV exposure, with the largest reduction between 300 nm and 400 nm. A corresponding change in the surface morphology of the nanotubes visible in the FESEM images also occurs. However, the magnitude of the change in reflectance and the influence of further UV exposure on the reflectance differs for each sample.

The spray-on sample was visibly damaged and flaking off after 17 kJ of UV exposure. This is not surprising since this coating incorporates a binder that we expect to be heat and UV sensitive. The NIST VACNT exposure was limited to 5 kJ by a failure in the UV laser system. We include the measurements since the reduction in reflectivity is apparent even with the lower exposure.

The FESEM images of the surface of the sample and measured spectral hemispherical reflectances before and after UV exposure for each sample are shown in Figures 2–7.

For each sample, the non-irradiated surface appeared to be a visually uniform coating. As the UV laser irradiance was increased, a noticeable coarsening of the top surface morphology was observed in each sample.

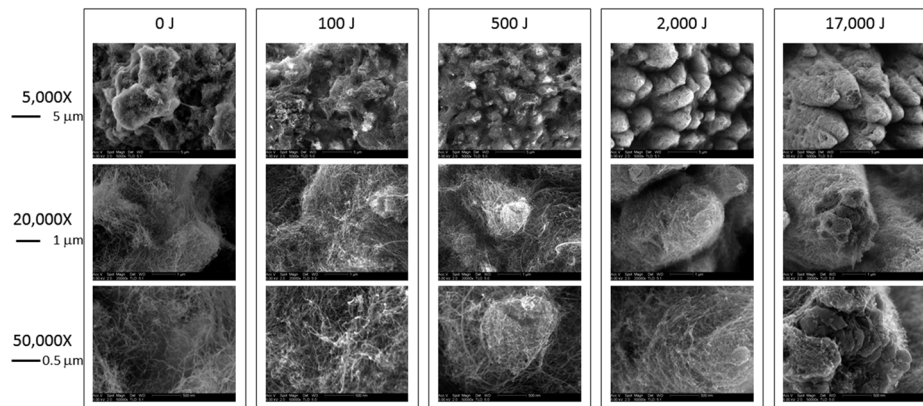


FIG. 2. FESEM images of the top surface of the commercial spray-on carbon nanotube coating after increasing exposure to UV laser light. Rows show images with increasing magnification, 5000X, 20000X, 50000X. Columns show images taken after increasing UV exposure. The left column shows images taken before any UV exposure (0 J).

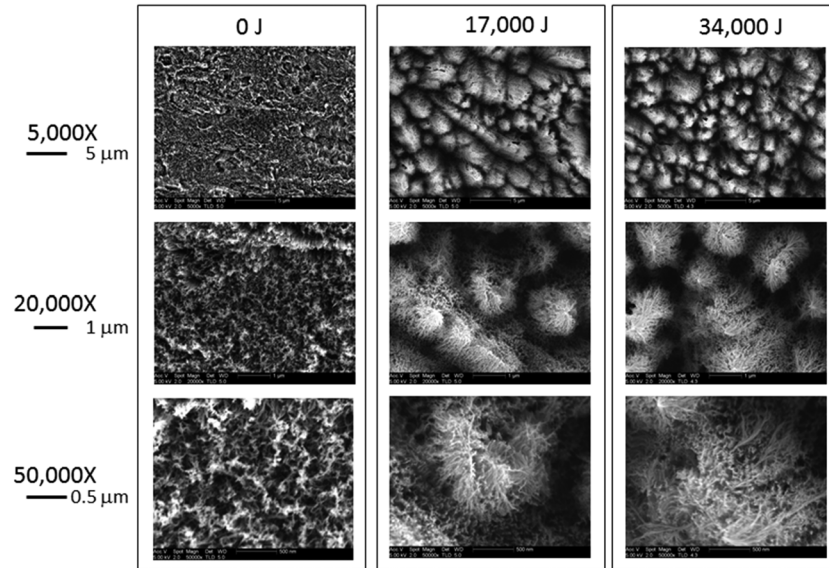


FIG. 3. FESEM plan view images of the top surface of the commercial VACNT coating on Al substrate after increasing exposure to UV laser light. Rows show images with increasing magnification, 5000X, 20000X, 50000X. Columns show images taken after increasing UV exposure. The left column shows images taken before any UV exposure (0 J).

IV. DISCUSSION

The images and reflectance measurements show a flattening of the reflectance spectrum associated with an altered surface morphology. For the VACNT samples, initially the surface has a uniform, higher density and so is higher reflectance than the bulk VACNTs. We speculate that the laser irradiation removes a top crust consisting of entangled CNTs and amorphous carbon to expose the VACNT forest below and may also result in agglomeration of the nanotube tips.

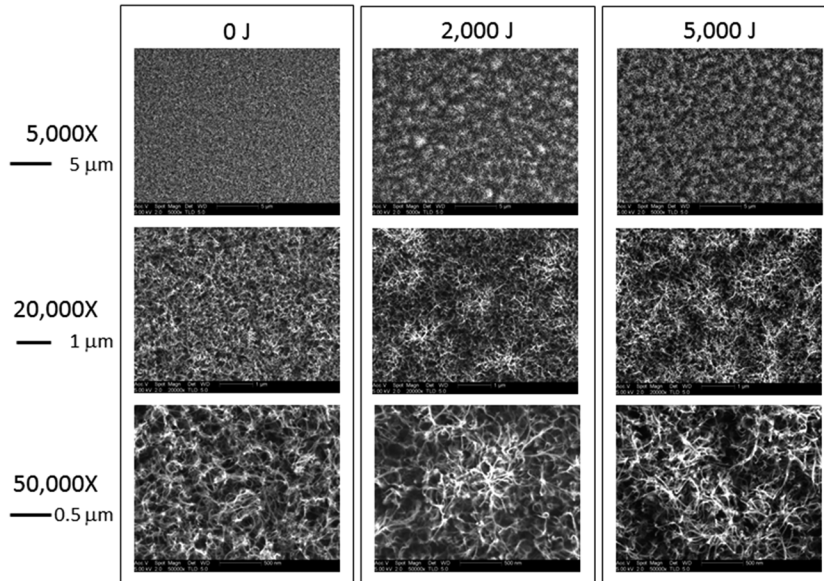


FIG. 4. FESEM plan view images of the top surface of the VACNT coating on silicon after increasing exposure to UV laser light. Rows show images with increasing magnification, 5000X, 20000X, 50000X. Columns show images taken after increasing UV exposure. The left column shows images taken before any UV exposure (0 J).

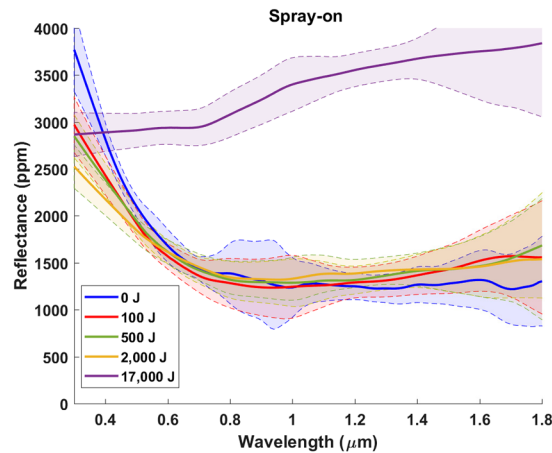


FIG. 5. Reflectance vs. wavelength for the commercial spray-on carbon nanotube coating before UV exposure (0 J) and after 100 J, 500 J, 2,000 J, and 17,000 J of UV exposure. The shaded areas indicate the $k = 2$ uncertainty for each measurement. At 17,000 J exposure, the coating was visibly damaged and flaking off.

VACNT growth is initially randomly oriented, until the growth forces a self-oriented vertical alignment.^{11,17} Crust layers of tangled CNTs¹⁷ and of amorphous carbon^{18,19} can be formed on top of the VACNTs during growth. When the crust layer is removed so that incident radiation impinges directly on the VACNT surface, the reflectance of the VACNTs decreases.¹¹ It has been shown that the crust layer can be removed via an oxygen plasma treatment, and that the oxygen plasma treatment also induces agglomeration of the tips that further reduces the reflectance, possibly because the tips are attracted by charging of nanotube defects and functionalization.¹¹ It has also been shown that amorphous carbon can be removed on single-wall carbon nanotubes via UV laser assisted oxidation¹⁴ or thermally.²⁰ We believe that the effect seen here is a removal of a crust layer, like that shown in Tomlin, *et al.*¹¹ due to a combination of thermal heating and UV laser assisted oxidation of the surface crust. It is important to note that the impact of the irradiance varies with the nanotube deposition process. The carbon nanotubes on the commercial spray-on sample are not vertically aligned and are mixed with a binder that we expect to be heat and UV sensitive. An understanding of the processes responsible for the changes to spray-on coating would require knowledge of the binder's chemical composition. However, the physical processes²¹ described in previous measurements on single wall CNTs in vacuum¹⁴ and multi-wall CNTs in nitrogen¹³ can be used to examine what is seen here on vertically aligned multi-wall CNTs in vacuum.

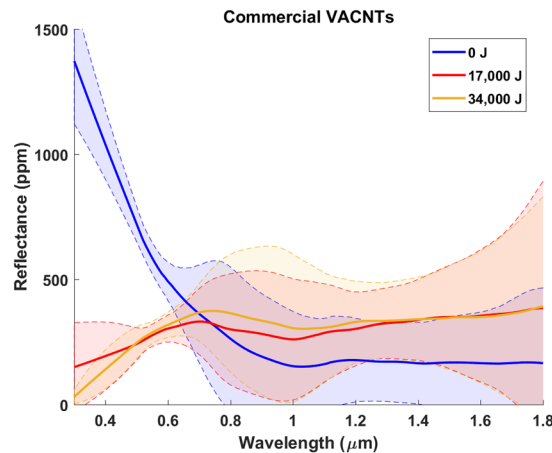


FIG. 6. Reflectance vs. wavelength for commercial vertically aligned carbon nanotube coating on Al substrate before UV exposure (0 J) and after 17,000 J and 34,000 J. The shaded areas indicate the $k = 2$ uncertainty for each measurement.

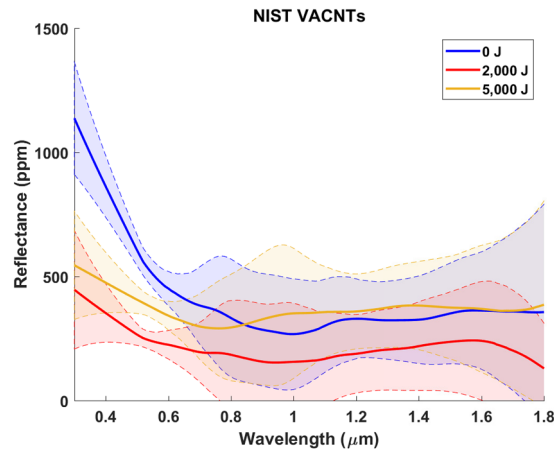


FIG. 7. Reflectance vs. wavelength for vertically aligned carbon nanotube coating grown in-house before UV exposure (0 J) and after 2,000 J and 5,000 J. The shaded areas indicate the $k = 2$ uncertainty for each measurement.

The 248 nm UV photons excite the π plasmon in the CNTs, which has a broad absorption peak centered at ~ 248 nm.¹² The excitation leads to a resonant enhancement of the photons resulting in an efficient transfer of energy to and heating of the CNTs.²¹ When oxygen is present, this energy transfer “cleans” the CNTs by assisting in oxidation of the amorphous carbon.^{14,21} Additionally, rapid thermal cycling caused by laser radiation has been shown to locally melt CNTs¹³ and cause structural defects in the outer walls of the VACNTs.^{22,23} The rapid, high temperature rise caused by the UV laser may vaporize the crust and expose the lower reflectivity VACNTs underneath. Since the residual water and O_2 gas in the vacuum can lead to UV stimulated etching,¹⁴ we believe both the thermal and photochemical mechanisms are likely to be present. The surface morphology change is evident in Figures 2–4.

We created a thermal model in COMSOL to explore the possible heating mechanism on multi-wall VACNTs. We found that a thermal model of pure VACNTs suggest that heating of VACNTs alone cannot account for loss of carbon from the surface. However, a model of a thin crust of amorphous carbon on top of a forest of VACNTs shows that a crust of 50 nm or greater can be heated to temperatures on the order of the vaporization temperature of carbon. We present a model of the thermal behavior of a thin, amorphous carbon crust on VACNTs, representative of the two samples with VACNTs.

Finite element simulations were performed to predict the maximum temperature and rate of change of the temperature during a single laser pulse. An axisymmetric model was created, centered around the optical axis of the incident laser beam. As the penetration depth of the 248 nm light is around 10 nm,¹⁶ we modeled the heat input, Q , as a surface heat absorption. The temporal profile was Gaussian with a full width at half maximum of 22 ns. The heat input and transport equations, as well as the thermal properties used are given in Table I along with references. The model consisted of a Si substrate 500 μm thick and 40 mm in diameter with a 450 μm thick VACNT layer modeled as a uniform layer on top. Later, an additional 100 nm surface layer of amorphous carbon (aC) was added. The interface between the VACNT layer and the Si substrate was modeled with a thermal contact conductance, h .²⁴ Radiative heat loss from the VACNTs and Si substrate was a small contribution but was included with emissivities of these layers given as 1 and 0.7, respectively.²⁵

The temperature dependent heat capacity of the VACNT was interpolated from values taken from Huang *et al.*,²⁶ where it was found to deviate from graphite at elevated temperatures due to enhanced boundary and point defect scattering. The density of the VACNTs was estimated from the measured fill factor of our VACNTs. Values for heat capacity germane to our MWCNTs are difficult to verify given the wide range of MWCNT arrangements and configurations, as well as the limited amount of experimental data that exists at high temperatures. Therefore, we attempted to use a reasonable lower bound estimate. The thermal conductivity, k , of CNTs has a wide range in the literature as it depends strongly on process conditions, defects, and degree of nanotube interconnection. Therefore, a range

TABLE I. Parameters, equations, and values used for finite element simulations. C_p is the specific heat, ρ is the density, k is the thermal conductivity, T is the temperature, r is the radius of the sample, u is the unit spatial vector and σ is the $1/e^2$ laser pulse width.

Parameter	Equations and Values	Ref.												
Heat Transport Equation	$\rho C_p \frac{\partial T}{\partial t} + \rho C_p \mathbf{u} \cdot \nabla T - \nabla k T = Q$	33												
Heat input, Q (W/m ²)	$\frac{E_0}{\sqrt{2\pi}\sigma(\pi r^2)} e^{-(t-t_0)^2/2\sigma^2} = Q$													
$C_p(T)$, VACNT/aC	<table border="1"> <thead> <tr> <th>Temperature (K)</th> <th>Value (J/(kg K))</th> </tr> </thead> <tbody> <tr><td>250</td><td>500</td></tr> <tr><td>300</td><td>700</td></tr> <tr><td>400</td><td>850</td></tr> <tr><td>500</td><td>950</td></tr> <tr><td>700</td><td>1000</td></tr> </tbody> </table>	Temperature (K)	Value (J/(kg K))	250	500	300	700	400	850	500	950	700	1000	26
Temperature (K)	Value (J/(kg K))													
250	500													
300	700													
400	850													
500	950													
700	1000													
ρ , VACNT/aC	0.05 (g/cm ³)													
k , VACNT	1-3000 (W/m-K)	26,34,35												
h , VACNT/Si interface	1×10^6 (W/(m ² -K))	24												
$C_p(T)$, Si	$(0.158 + 3.13 \times 10^3 \times T - 5.60 \times 10^{-6} \times T^2 + 5.22 \times 10^{-9} \times T^3 - 2.40 \times 10^{-12} \times T^4 + 4.29 \times 10^{-16} \times T^5)$ J/(g-K)	28												
ρ , Si	$(2330 + 0.484 \times T + 1.98 \times T^2)$ kg/m ³	29												
k , Si	$(95.44 - 0.0969 \times T + 3.27 \times 10^5 \times T^2)$ W/(m-K)	30,31												

of values were used. Similarly, literature values for k for aC exist over a range and is dependent largely on density.²⁷ The temperature dependent thermophysical property values of the Si substrate²⁸⁻³¹ are also given in Table I and are similar those used in Simonds, et al.^{32,33}

Figure 8 shows results of the surface temperature at the center of the laser beam interaction with the VACNT of the simple model where we assume only VACNT on a Si substrate with the thermal conductivity of the VACNT varying over the range typically found in the literature for CNT bundles or mats.^{26,35,36} A curve with $k = 3000$ W/(m K), which is the value measured for a single CNT is shown for comparison.³⁴ What these curves suggest is that a low thermal conductivity of the VACNT does not account for loss of carbon from the surface because the VACNTs alone do not reach the evaporation temperature of carbon in a vacuum (4000 ± 1200 K).³⁷ As an extreme, we simulated a value of $k = 001$ W/(m K) which is an indefensibly low value 3 orders of magnitude below anything found in the literature. Only in that case does the predicted temperature rise at the surface asymptote to around 3000 °C, which is the lower end of the temperature range for evaporation of carbon in a vacuum. We also modeled the temperature rise of shorter VACNTs grown on an Al substrate and found no significant difference in the temperature rise.

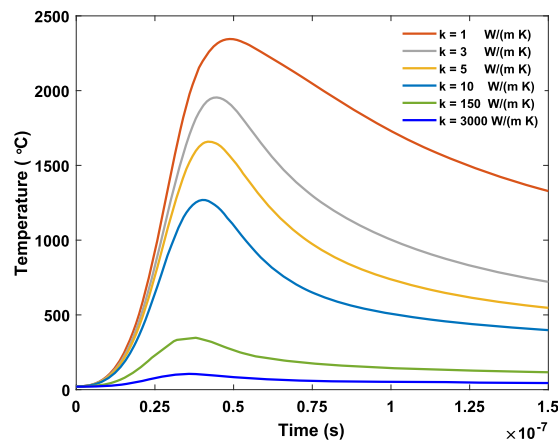


FIG. 8. Finite element temperature simulation of VACNT on silicon, varying thermal conductivity of VACNT.

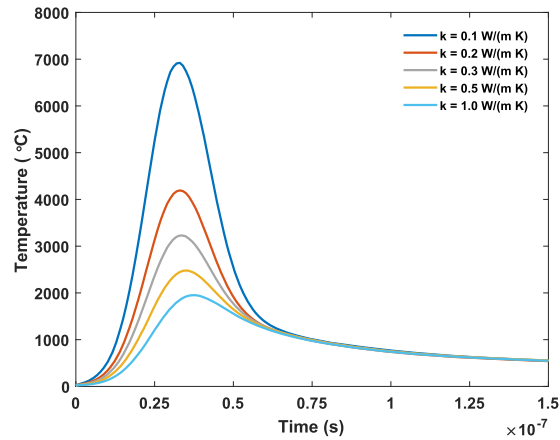


FIG. 9. Finite element temperature simulation of VACNT on silicon, with an aC crust layer added. The thermal conductivity of the VACNT is held fixed at 5 W/(m K). For these curves, the thermal conductivity of the VACNT was held fixed at 5 W/(m K). Note that as the crust begins to vaporize the vaporization will flatten the temperature profile. This effect is not included but will not impact whether the crust initially reaches the vaporization temperature.

Figure 9 shows the results obtained after we add a 100 nm thick aC crust layer to the surface of the VACNT in the model. When we vary the thermal conductivity of the aC layer in the model over the range found in the literature, we find that the surface temperature can rise significantly and reaches the temperature range for evaporation of carbon in a vacuum. Furthermore, a similar temperature range can also be achieved if a thermal contact resistance of similar order of magnitude as that found at the CNT/Si interface is included. As this aC crust layer is so much thinner than the VACNT layer, it is not surprising that these two regimes elicit similar behaviors. A combination of these two situations could exist. Therefore, we believe that a plausible explanation of the UV VACNT purification is that the early pulses are absorbed in a relatively thermally resistance surface region containing amorphous porous carbon. Such a change in surface morphology is seen in our FESEM images.

A 100 nm aC crust is relatively thick and should be detectable. To obtain an edge-on SEM image that would allow comparison of the surface crust before and after laser irradiation, the VACNTs were scraped off across the interface between the irradiated area and the area on the sample that was not

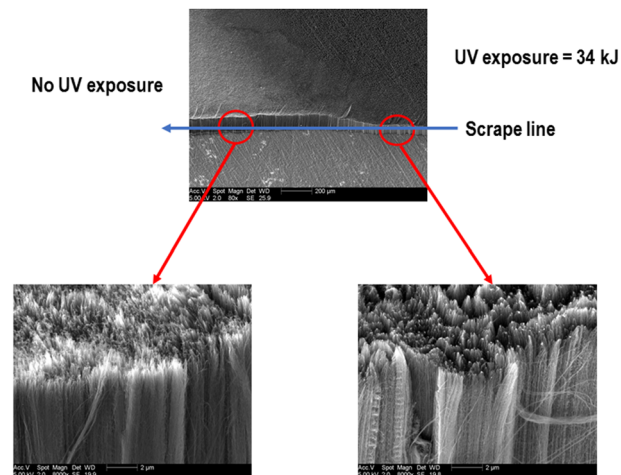


FIG. 10. Edge-on image of VACNTs on Al on area with no UV exposure (left) and UV exposure (right). The top image shows the visible contrast between the unexposed and exposed regions. A reduction in the height of the nanotubes, indicative of loss of material on the surface, is evident. The surface of the un-exposed VACNT's shows entangled CNT tips but no apparent layer of aC.

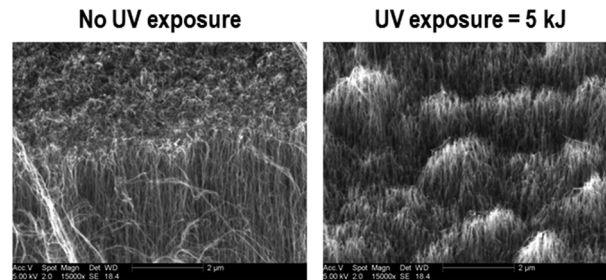


FIG. 11. Edge-on image of NIST in-house VACNTs on area with no UV exposure (left) and UV exposure (right). There was no significant contrast between the unexposed and exposed regions. The surface of the un-exposed VACNT's shows entangled CNT tips but no apparent layer of aC.

irradiated, and the exposed edge was imaged. While the height of the irradiated nanotubes has clearly been reduced in the irradiated area on one of the samples, indicating loss of material from the surface of the VACNTs, an amorphous carbon crust like that modeled is not apparent in the unexposed area, although entangled CNT tips are (Figures 10 and 11). It is plausible that there is a similar heating and vaporization in the entangled CNT crust; however, the conductive interface of an entangled CNT crust is very difficult to model as there are multiple, varying thermal contacts.

V. SUMMARY

We have shown that UV laser exposure can be used to flatten the spectral response of vertically aligned carbon nanotube coatings, making the darkest, most spectrally broadband absorbers currently available even darker at short wavelengths. All though we can not definitively state the process leading to the changes, we believe the effect is attributable to a combination of the heating and vaporization of an amorphous carbon or entangled CNT crust on top of the VACNTs and UV stimulated etching from residual water and O₂ gas. Both processes are driven by resonant absorption near 248 nm.

- ¹ E. Theocharous, C. Engtrakul, A. C. Dillon, and J. Lehman, *Applied Optics* **47**(22), 3999–4003 (2008).
- ² J. Lehman, A. Steiger, N. Tomlin, M. White, M. Kehrt, I. Ryger, M. Stephens, C. Monte, I. Mueller, J. Hollandt, and M. Dowell, *Opt Express* **24**(23), 25911–25921 (2016).
- ³ N. A. Tomlin and J. H. Lehman, *Optics Letters* **38**(2), 175–177 (2013).
- ⁴ Z. C. D. Harber, G. Drake, K. Heuerman, G. Kopp, J. Rutkowski, H. Passe, M. Smith, P. Smith, J. Sprunck, E. Richard, N. Tomlin, M. Stephens, M. White, C. Yung, and J. Lehman, in American Meteorological Society (Seattle, 2017).
- ⁵ W. H. Swartz, L. P. Dyrdur, S. R. Lorentz, D. L. Wu, W. J. Wiscombe, S. J. Papadakis, P. M. Huang, E. L. Reynolds, A. W. Smith, and D. M. Deglau, presented at the 2015 IEEE International Geoscience and Remote Sensing Symposium (IGARSS), 2015 Proceedings 5300–5303.
- ⁶ K. Mizuno, J. Ishii, H. Kishida, Y. Hayamizu, S. Yasuda, D. N. Futaba, M. Yumura, and K. Hata, *Proc. Natl. Acad. Sci. U S A* **106**(15), 6044–6047 (2009).
- ⁷ D. P. Osterman, S. Collins, J. Ferguson, W. Good, T. Kampe, R. Rohrschneider, and R. Warden, *Proc. SPIE* **9978**, 99780E (2016).
- ⁸ J. G. Hagopian, S. A. Getty, M. Quijada, J. Tveekrem, R. Shirri, P. Roman, J. Butler, G. Georgiev, J. Livas, C. Hunt, A. Maldonado, S. Talapatra, X. Zhang, S. J. Papadakis, A. H. Monica, and D. Deglau, *Proc. SPIE* **7761**, 77610F (2010).
- ⁹ M. A. Quijada, M. Wilson, E. Waluschka, and C. R. McClain, *Proc. SPIE* **8153**, 81530T (2011).
- ¹⁰ M. R. Dury, T. Theocharous, N. Harrison, N. Fox, and M. Hilton, *Optics Communications* **270**(2), 262–272 (2007).
- ¹¹ N. A. Tomlin, A. E. Curtin, M. White, and J. H. Lehman, *Carbon* **74**, 329–332 (2014).
- ¹² T. Pichler, M. Knupfer, M. S. Golden, J. Fink, A. Rinzler, and R. E. Smalley, *Physical Review Letters* **80**(21), 4729–4732 (1998).
- ¹³ Á. P. d. Pino, E. György, L. Cabana, B. Ballesteros, and G. Tobias, *Journal of Applied Physics* **115**(9), 093501 (2014).
- ¹⁴ K. E. Hurst, A. C. Dillon, S. Yang, and J. H. Lehman, *The Journal of Physical Chemistry C* **112**(42), 16296–16300 (2008).
- ¹⁵ Z. Guofang, I. Takayuki, H. Kotaro, F. Yukio, O. Iwao, and K. Hiroshi, *Japanese Journal of Applied Physics* **44**(4R), 1558 (2005).
- ¹⁶ J. Lehman, C. Yung, N. Tomlin, D. Conklin, and M. Stephens, *Applied Physics Reviews* **5**(1), 011103 (2018).
- ¹⁷ Y. Won, Y. Gao, R. G. d. Villoria, B. L. Wardle, T. W. Kenny, and K. E. Goodson, presented at the 13th InterSociety Conference on Thermal and Thermomechanical Phenomena in Electronic Systems, 2012 Proceedings 1070–1076.
- ¹⁸ K. B. K. Teo, M. Chhowalla, G. A. J. Amaratunga, W. I. Milne, D. G. Hasko, G. Pirio, P. Legagneux, F. Wyczisk, and D. Pribat, *Applied Physics Letters* **79**(10), 1534–1536 (2001).
- ¹⁹ Q. N. Pham, L. S. Larkin, C. C. Lisboa, C. B. Saltonstall, L. Qiu, J. D. Schuler, T. J. Rupert, and P. M. Norris, *Physica Status Solidi (A)* **214**(7), 1600852 (2017).
- ²⁰ P. Corio, P. S. Santos, M. A. Pimenta, and M. S. Dresselhaus, *Chemical Physics Letters* **360**(5), 557–564 (2002).

- ²¹ A. G. Van der Geest, K. E. Hurst, N. D. Bronstein, J. H. Lehman, and M. T. Lusk, *Physical Review B* **81**(11), 115440 (2010).
- ²² E. György, Á. Pérez del Pino, J. Roqueta, B. Ballesteros, L. Cabana, and G. Tobias, *Journal of Nanoparticle Research* **15**(8), 1852 (2013).
- ²³ G. Singh, P. Rice, K. E. Hurst, J. H. Lehman, and R. L. Mahajan, *Applied Physics Letters* **91**(3), 033101 (2007).
- ²⁴ T. Tong, Y. Zhao, L. Delzeit, A. Kashani, M. Mayyappan, and A. Majumdar, *IEEE Trans. Components Packag. Technol.* **30**(1), 92–100 (2007).
- ²⁵ S. Tsutomu, *Japanese Journal of Applied Physics* **6**(3), 339 (1967).
- ²⁶ X. Huang, J. Wang, G. Eres, and X. Wang, *Carbon* **49**(5), 1680–1691 (2011).
- ²⁷ A. J. Bullen, K. E. O'Hara, D. G. Cahill, O. Monteiro, and A. v. Keudell, *Journal of Applied Physics* **88**(11), 6317–6320 (2000).
- ²⁸ P. D. Desai, *Journal of Physical and Chemical Reference Data* **15**(3), 967–983 (1986).
- ²⁹ Z. Zhou, S. Mukherjee, and W.-K. Rhim, *Journal of Crystal Growth* **257**(3), 350–358 (2003).
- ³⁰ Y. B. Magomedov and G. G. Gadjiev, *High Temperature* **46**(3), 422–424 (2008).
- ³¹ D. S. Beers, G. D. Cody, and B. Abeles, *Journal of Electronics and Control* **14**(3), 41–48 (1962).
- ³² B. J. Simonds, A. Teal, T. Zhang, J. Hadler, Z. Zhou, S. Varlamov, and I. Perez-Würfl, in *SPIE LASE* (SPIE, 2016), Vol. 9735, pp. 8.
- ³³ B. S. Yilbas, *Laser Heating Applications: Analytical Modeling* (Elsevier, Waltham, MA, 2012).
- ³⁴ P. Kim, L. Shi, A. Majumdar, and P. L. McEuen, *Physical Review Letters* **87**(21), 215502 (2001).
- ³⁵ H.-L. Zhang, J.-F. Li, B.-P. Zhang, K.-F. Yao, W.-S. Liu, and H. Wang, *Physical Review B* **75**(20), 205407 (2007).
- ³⁶ E. A. Ali, H. L. Marcio, M. S. Edward, and H. B. Ray, *Nanotechnology* **21**(3), 035709 (2010).
- ³⁷ S. I. Kudryashov, A. A. Karabutov, and N. B. Zorov, *Mendelevov Communications* **8**(4), 151–152 (1998).